Supplementary Information:

Identifying *s*-wave pairing symmetry in single-layer FeSe from topologically trivial edge states

Zhongxu Wei[1,2#], Shengshan Qin[3,4#], Cui Ding[5,2], Jiangping Hu[6,3,4], Yujie Sun[1*], Lili Wang[2*] and Qi-Kun Xue[1,2,5*]

[1]Department of Physics, Southern University of Science and Technology, Shenzhen 518055, China

[2]State Key Laboratory of Low-Dimensional Quantum Physics, Department of Physics, Tsinghua University, Beijing 100084, China

[3]Kavli Institute of Theoretical Sciences, University of Chinese Academy of Sciences, Beijing 100049, China

[4]CAS Center for Excellence in Topological Quantum Computation, University of Chinese Academy of Sciences, Beijing 100049, China

[5]Beijing Academy of Quantum Information Sciences, Beijing 100193, China

[6]Beijing National Research Center for Condensed Matter Physics, and Institute of Physics, Chinese Academy of Sciences, Beijing 100190, China

#These authors contributed equally to this work.

*email: sunyj@sustech.edu.cn; liliwang@mail.tsinghua.edu.cn; xueqk@sustech.edu.cn

Supplementary Note 1: Fitting of Tunneling Spectra

We try to extract superconducting energy gap by fitting the tunneling spectra with Dynes formula. Here, we take the blue spectrum at the bottom of Figure 3b in the main text as an example. Before fitting, the normalization is performed by dividing the raw spectrum by its background (blue solid and red dashed curves in Figure S1a). The background is extracted from a quintic polynomial fit to the conductance for |V| > 30 mV. The normalized spectrum, denoted by the blue circles in Figure S1b, still has a pair of coherence peaks with slightly different intensities. Such electron-hole asymmetry, which is common in iron-based superconductors, may be caused by the band-edge effect due to the relatively shallow band[1,2]. The normalized spectrum is then fitted by the Dynes formula:

$$\frac{\mathrm{d}I}{\mathrm{d}V} \propto \int_{-\infty}^{+\infty} \mathrm{d}E \int_0^{2\pi} \frac{1}{2\pi} \mathrm{d}\theta \frac{\partial f(E+eV)}{\partial V} \left| \mathrm{Re}\left(\frac{E-i\Gamma}{\sqrt{(E-i\Gamma)^2-\Delta^2(\theta)}} \right) \right|,$$

where f is the Fermi-Dirac function, Γ is a broadening factor due to the finite quasi-particle lifetime. Since the angle-resolved photoemission spectroscopy measurement has demonstrated that the superconducting gap of single-layer FeSe is moderately anisotropic and a best fit of the gap as a function of angle includes $\cos 2\theta$ and $\cos 4\theta$ terms[3], we take a gap function of

$$\Delta(\theta) = \Delta_0 \left[1 - p_1 \left[1 - \cos\left[4\left(\theta - \frac{\pi}{4}\right)\right]\right] - p_2 \left[1 - \cos\left[2\left(\theta - \frac{\pi}{4}\right)\right]\right]\right],$$

where p_1 and p_2 are the weight of $\cos 4\theta$ and $\cos 2\theta$ terms, respectively.

Based on the above formula, the normalized data is well fitted, as shown by the red curve in Figure S1b. More fitting results of normalized tunneling spectra with different superconducting gap magnitude are shown in Figure S1c, and corresponding fitting parameters are summarized in Table S1. Under such criteria, we obtain the evolution of the gap magnitude near the (11) and (01) edges (Figures 2a and 3a in the main text), as shown in Figures S1d and S1e respectively. It is found that gap magnitude decreases with moving close to the edge.

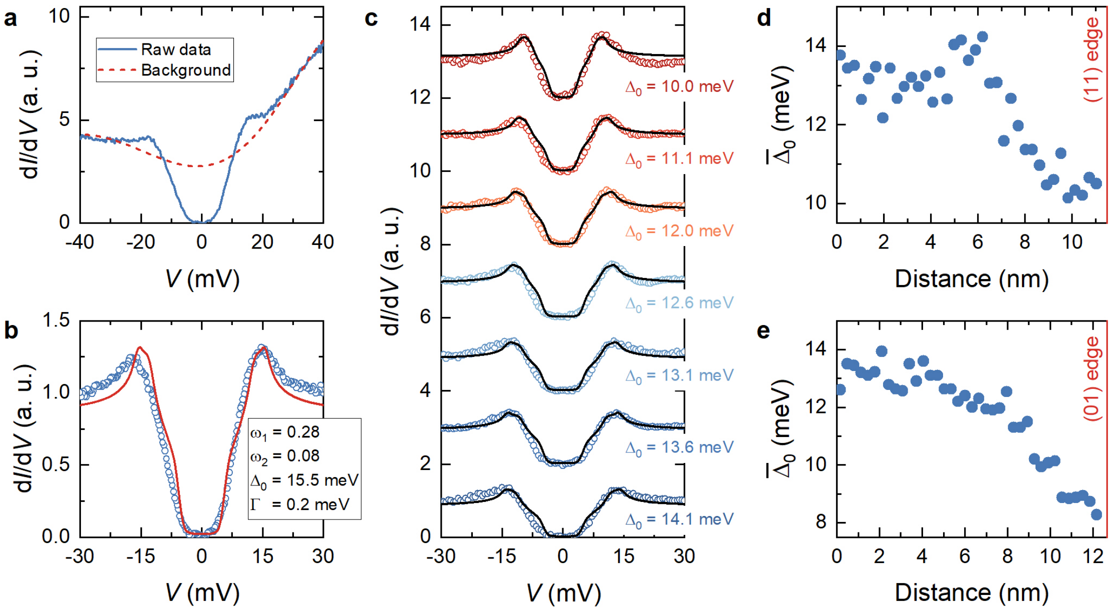

Figure S1 | Fitting of tunneling spectra. a, A copy of the blue spectrum at the bottom of Figure 3b in the main text, and its background (red dashed curve). **b**, Normalized data (blue circles) and the fitting result (red curve). **c**, Fitting results of normalized tunneling spectra with various superconducting gap magnitude. **d-e**, Averaged gap magnitude as a function of the distance to the (11) and (01) edges.

Table S1 | Fitting parameters of the spectra shown in Figure S1c.

No.	Δ (meV)	Γ (meV)	p_1	p_2
1	10.0	0.10	0.28	0.09
2	11.1	0.15	0.29	0.09
3	12.0	0.10	0.28	0.10
4	12.6	0.20	0.25	0.09
5	13.1	0.15	0.27	0.09
6	13.6	0.15	0.27	0.10
7	14.1	0.15	0.29	0.08

Supplementary Note 2: Additional data for the (01) edge

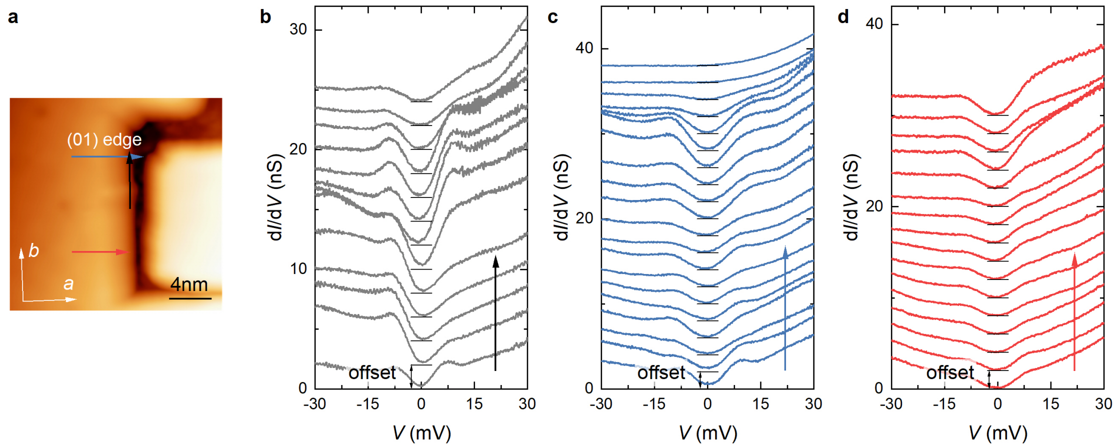

Figure S2 | Electronic states at the (01) edge of single-layer FeSe. a, STM topographic image (V_s = 0.5 V, I_t = 100 pA) of the (01) edge. **b-d**, Tunneling spectra (V_s = 50m V, I_t = 500 pA) measured along the black (**b**), blue (**c**) and red (**d**) arrows in **a**. The top two spectra in **c** are taken on the $SrTiO_3$(001) surface. These is no significant change in zero-bias conductance of these spectra.

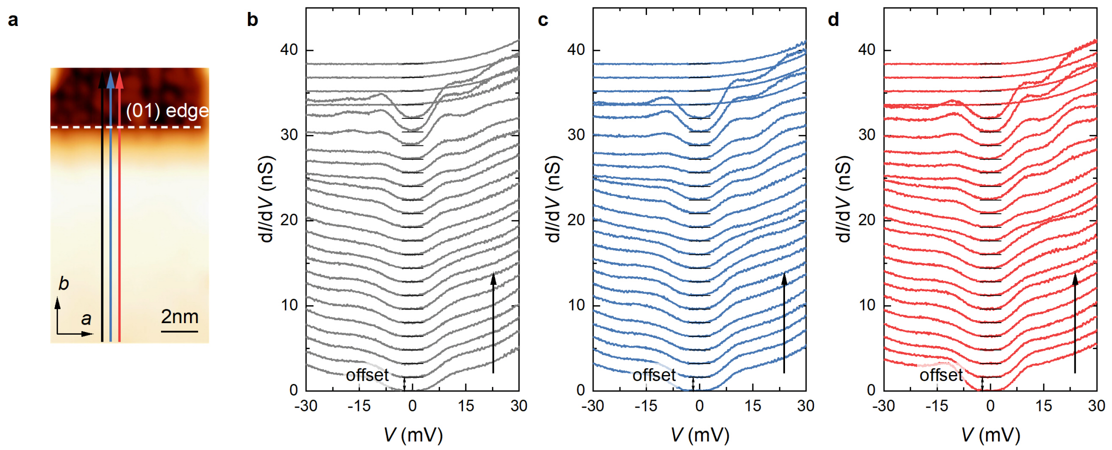

Figure S3 | Electronic states at the (01) edge of single-layer FeSe. a, STM topographic image (V_s = 1 V, I_t = 50 pA) of the (01) edge. **b-d**, Tunneling spectra (V_s = 50m V, I_t = 500 pA) measured along the black (**b**), blue (**c**) and red (**d**) arrows in **a**. The top four spectra in **b-d** are taken on the $SrTiO_3$(001) surface. The zero-bias conductance is almost position-independent.

Supplementary Note 3: Additional data for the corner between (11) and $(1\bar{1})$ edges

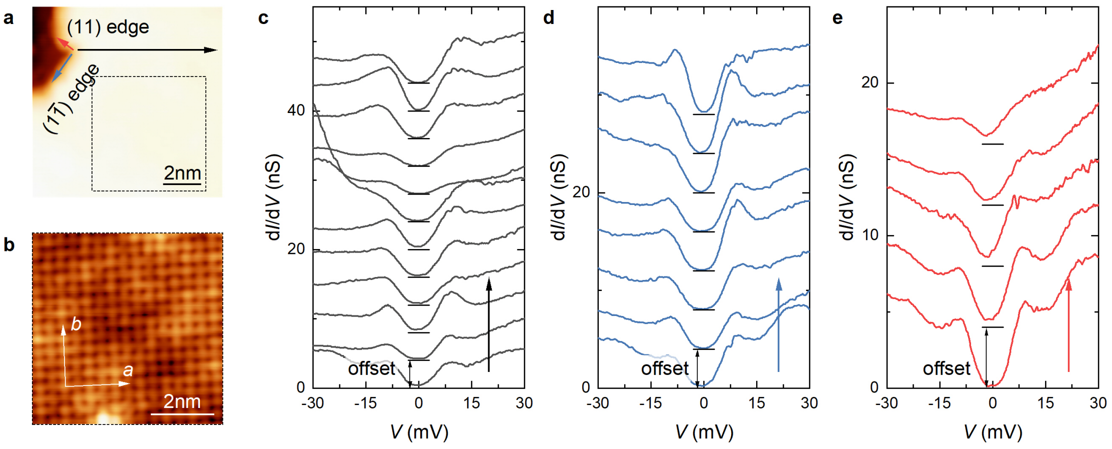

Figure S4 | Electronic states at the corner between (11) and $(1\bar{1})$ edges. a, STM topographic image (V_s = 1 V, I_t = 50 pA) of the corner between (11) and $(1\bar{1})$ edges. **b**, Atomically resolved image (V_s = 50 mV, I_t = 500 pA) taken from the area outlined by the black dashed box in **a**. **c-e**, Tunneling spectra (V_s = 50 mV, I_t = 500 pA) measured along the black (**c**), blue (**d**) and red (**e**) arrows in **a**. There is no trace of Majorana zero-energy mode.

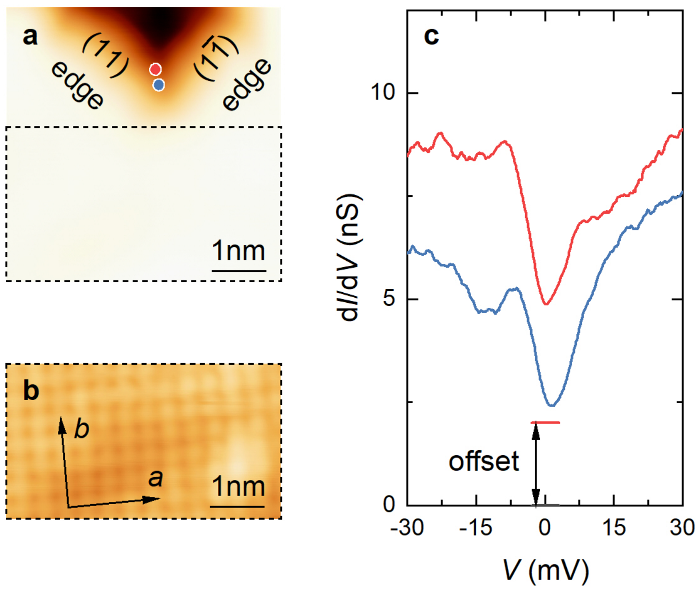

Figure S5 | Electronic states at the corner between (11) and $(1\bar{1})$ edges. a, STM topographic image (V_s = 1 V, I_t = 50 pA) of the (11) & $(1\bar{1})$ corner. **b**, Atomically resolved image (V_s = 50 mV, I_t = 500 pA) taken from the area outlined by the black dashed box in **a**. **c**, Tunneling spectra (V_s = 50 mV, I_t = 500 pA) collected at the locations marked by the corresponding colored circles in **a**. The zero-bias conductance peak as supposed for $s_{\pm}$-pairing is missing.

Supplementary Note 4: Simulations for the possible influence of the substrate on the experimental observations

We carry out numerical simulations for the possible influence of the STO substrate on the experimental observations of the topological edge/corner modes. In the calculations, instead of using the genuine but complicated model Hamiltonian for the single-layer FeSe which involves all the five *d* orbitals from Fe, we adopt a simple toy model which captures the key topological properties of the sign-changed $s_{\pm}$-wave pairing state. In the toy model, we consider one single *s* orbital at each Fe lattice site and the normal-state Hamiltonian reads as

$$H_0(\boldsymbol{k}) = [2t(\cos k_x + \cos k_y) - \mu]s_0\sigma_0 - 2R(\sin k_x\, s_2 + \sin k_y\, s_1)\sigma_3 + 4t' \cos\frac{k_x}{2}\cos\frac{k_y}{2}\, s_0\sigma_1,$$

where s_i and σ_i are the Pauli matrices in the space of the electron spin and two Fe sublattices, respectively. Notice that k_x and k_y are defined according to the primitive lattice translations along the next-nearest-neighbour Fe-Fe directions, *i.e.* the (10) and (01) directions in the main text. In $H_0(\boldsymbol{k})$, μ is the chemical potential, t (t') is the hopping between the next-nearest-neighbour (nearest-neighbour) Fe lattice sites, and *R* is the Rashba-type spin-orbit coupling between the next-nearest-neighbour Fe lattice sites which arises from the mismatch between the Fe lattice sites and the inversion center. $H_0(\boldsymbol{k})$ respects the symmetry group of the single-layer FeSe and the corresponding band structures are plotted in Figure S6a. For the superconducting part, we consider the following *s*-wave pairing

$$H_{pair}(\boldsymbol{k}) = [\Delta_0 + 2\Delta_1(\cos k_x + \cos k_y)]is_2\sigma_0,$$

where Δ_0 is the onsite pairing and Δ_1 is pairing between the next-nearest-neighbour Fe lattice sites. By tuning the relative magnitude of Δ_0 and Δ_1, we can control the pairing signs on the different Fermi surfaces in $H_0(\boldsymbol{k})$. As shown in Figure S6b, we choose a set of parameters ($\{\Delta_0, \Delta_1\} = \{0.48, 0.2\}$) to simulate the sign-changed $s_{\pm}$-wave pairing state in the iron-based superconductors. For the state in Figure S6b, we calculate the superconducting edge modes on the (10) edge and the corner modes between the (11) and $(1\bar{1})$ edges directly and show the results in Figures S6c and S6d. Obviously, the above simple model well captures the main features of the second-order topological superconductivity in the sign-changed $s_{\pm}$-wave pairing state in the iron-based superconductors predicted in Ref. [4].

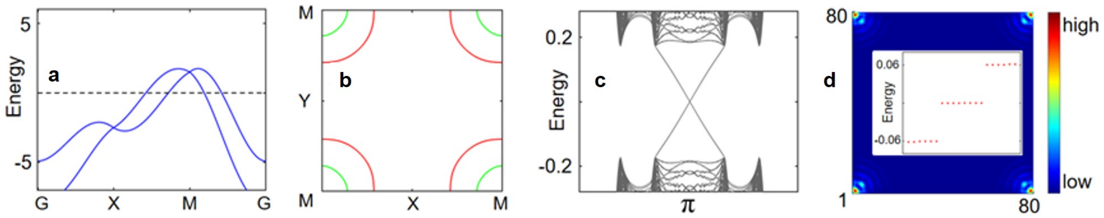

Figure S6 | Simulations for the topological edge/corner modes. a shows the band structures calculated from $H_0(\boldsymbol{k})$ with parameters $\{t, t', R, \mu\} = \{-1.0, 0.4, 0.5, 2.5\}$ with the Fermi energy labeled by the dashed line. **b** shows the Fermi surfaces (colored lines) corresponding to the condition in **a**, and the different colors represent the different pairing signs on the Fermi surfaces corresponding to the superconducting pairing in $H_{pair}(\boldsymbol{k})$ with $\{\Delta_0, \Delta_1\} = \{0.48, 0.2\}$. The superconducting edge/corner modes corresponding to the condition in **b** are presented in **c**/**d**. **c** shows the edge modes near $k = \pi$ on the (10) edge. Notice that the Dirac edge modes are twofold degenerate. **d** shows the wavefunction profile for the corner Majorana modes with open boundary conditions along the (11) and $(1\bar{1})$ directions, and the inset shows the low-energy spectrum.

In the following, we utilize the above model to simulate the influence of the substrate on the experimental observations, and we adopt the real-space configurations shown in Figures S7a-S7c in the simulations. The total Hamiltonian for the system reads

$$H_{total}(\boldsymbol{k}) = H_{sc}(\boldsymbol{k}) + H_n(\boldsymbol{k}) + H_{hyb}(\boldsymbol{k}).$$

In this equation, $H_{sc} = H_0 + H_{pair}$ is the toy-model superconducting Hamiltonian in the above, $H_n(\boldsymbol{k}) = 2t_n(\cos k_X + \cos k_Y) + V - \mu$ describes a simple square lattice with t_n being the nearest-neighbour hopping and V being the onsite energy. The hybridization between the superconducting and normal parts is depicted by H_{hyb} containing simply the nearest-neighbour hopping as indicated Figure S7c. In modeling the system, we choose proper $V = V_b$ to make the normal region beneath the superconductor metallic since charge transfer is believed to occur between FeSe and STO, and we make the other normal regions insulating ($V = V_n$), *i.e.* contribute no Fermi surface, as indicated in Figures S2-S3, Figure 4d in the main text, and Ref. [5].

We present the main numerical results in Figure S7. In the calculations, we consider $V_b = 6.0$ and $V_b = 5.0$ in the normal region beneath the superconductor, and in both cases H_n contribute an electron Fermi pocket near the Brillouin zone center. In the latter case, the normal region has larger electron Fermi pocket which almost compensates the hole Fermi pockets in the superconductor shown in Figures S6a and S6b. We also consider the strong ($t_h = 0.5$) and weak ($t_h = 0.2$) hybridization between the superconducting and normal layers. As shown in Figure S7, the topological edge/corner modes, especially the corner modes, can be weakened due to its leakage into the substrate; however, finite constant density of states (DOS) are still expected on the (10) edge as indicated in Figures S7d1-S7d4 and S7e1-S7e4. Similarly, a residual zero-bias peak is also expected at the corner between the (11) and $(1\bar{1})$ edges as indicated in Figures S7f1-S7f4 and S7g1-S7g4.

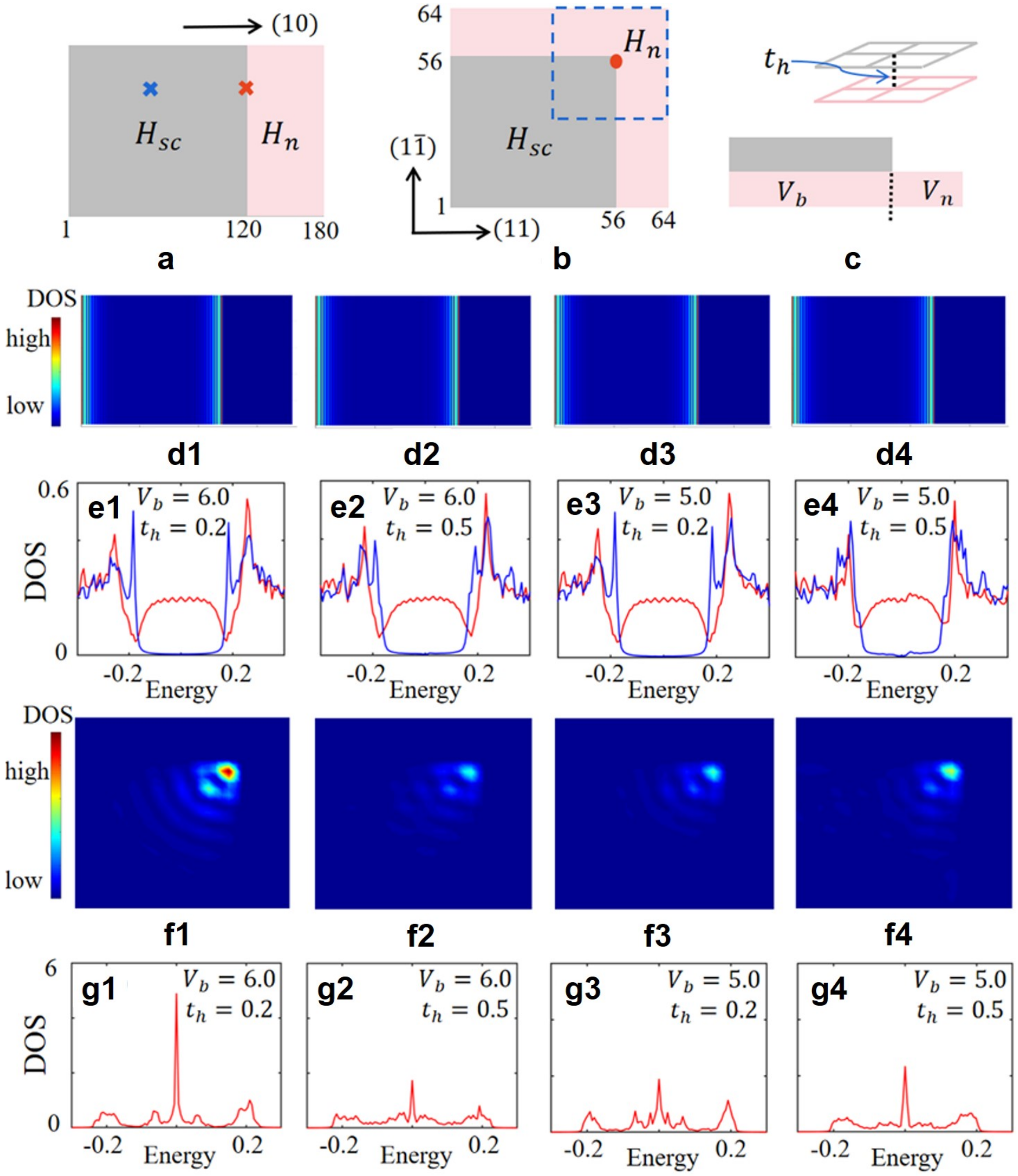

Figure S7 | Possible influence of the substrate on the experimental observations of edge/corner modes. **a** and **b** sketch the real-space configurations with which we simulate the influence of the substrate on the edge and corner modes respectively. In **a** we adopt open boundary condition in the (10) direction and periodic boundary condition in the (01) direction, and in **b** we adopt open boundary conditions both in the (11) and $(1\bar{1})$ directions. The gray (pink) part corresponds to the superconducting (normal) region, and the size of the lattice is marked in the figures. **c** shows the side view corresponding to **a** and **b**. Due to the charge transfer between the superconductor and the substrate, the normal region beneath the superconductor can have different onsite energy from the other regions, which is indicated by V_b and V_n in **c**. **d1**-**d4** show the simulations for the real-space zero-energy DOS of the superconducting edge modes in the configuration in **a**, and the figures share the same color bar. **e1-e4** present the local DOS at the location marked by × in **a**, and the colored lines in **e1-e4** are in accordance with the locations marked with the corresponding colors. **f1-f4** show the real-space zero-energy DOS of the superconducting corner modes in the region marked by the dashed line in **b**, and the figures share the same color bar. **g1-g4** present the local DOS at the corner marked by the red point in **b**. In the superconducting region described by H_{sc} we adopt the same parameters with these in Figure S6, in which case the region has a bulk superconducting gap about 0.2. In the normal region described by H_n, we set $t_n = -1.0$, and set $V_b = 6.0$ ($V_b = 5.0$) for the region beneath the superconductor in **d1-g1** and **d2-g2** (**d3-g3** and **d4-g4**) to make it metallic, and in other regions we set $V_n = 7.5$ to make them insulating. For the hybridization between the superconducting and normal parts described by H_{hyb}, we set $t_h = 0.2$ ($t_h = 0.5$) for the region beneath the superconductor in **d1-g1** and **d3-g3** (**d2-g2** and **d4-g4**).

As a comparison, we also calculate the experimental observations at the edge/corner corresponding to the sign-preserving *s*-wave pairing state in the presence of the substrate. It is found that the results are completely different from the sign-changed $s_{\pm}$-wave state, as shown in Figure S8. Obviously, a U-shape superconducting gap with no in-gap DOS is expected on the (10) edge, and no signature for the zero-bias peak is expected at the corner between the (11) and $(1\bar{1})$ edges.

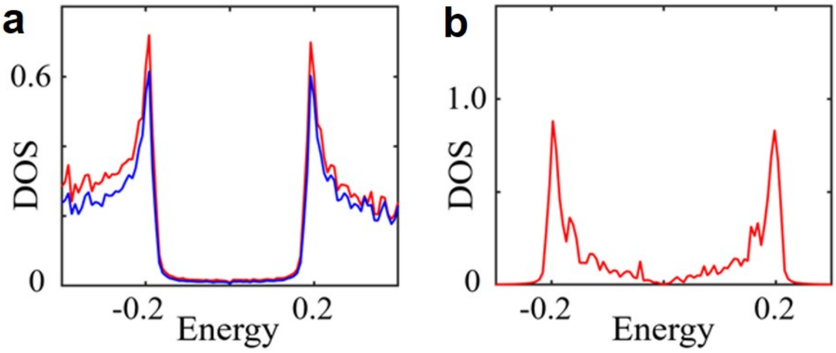

Figure S8 | Influence of the $SrTiO_3$ substrate on the experimental observations of edge/corner states. a and **b** show the local DOS at the (10) edge and at the corner between the (11) and $(1\bar{1})$ edges in the sign-preserving s-wave pairing state respectively. The colored curves in **a** are calculated at locations marked by the corresponding colored × in Figure S7a. The curve in **b** is calculated at the location marked by the red point in Figure S7b. In calculating **a** and **b**, we adopt the superconducting order parameters $\{\Delta_0, \Delta_1\} = \{0.2, 0.0\}$ in $H_{pair}(\boldsymbol{k})$, and the other parameters are all the same with these in Figure S7e4 and S7g4.

Finally, it is worth mentioning that although the model we adopted in the calculations is simpler compared to the actual FeSe/STO system, the results can still provide us important implications as the model captures the main physics near the Fermi energy. Therefore, it is reasonable to conclude that the topological edge/corner modes can serve as experimental observables to distinguish the pairing symmetry of the single-layer FeSe system even in the presence of the substrate.

Supplementary Note 5: Analysis of spectral weight of the normalized tunneling spectra

Z. Z. Ge et al. argues a nodeless *d*-wave pairing based on the observation of decreased gap magnitude and emergent conductance peak at the (01) edge but not at the (11) edge[6]. The conductance peak is located near the superconducting gap and can only be resolved after a normalization done by subtracting the spectrum far from the edge. In this work, however, we observe the decrease of Δ at both (01) and (11) edges (Figures 2c and 3c in the main text and Supplementary Figures S1d and S1e), which may be due to the lattice discontinuity (Figures 2a and 3a in the main text). In addition, we capture the conductance peak in normalized tunneling spectra at both (01) and (11) edges. Figure S9c shows a set of tunneling spectra measured along the black arrow in Figure S9a. Using the normalization method proposed by Ref. [6], that is, subtracting each spectrum (#1 ~ #23) from the spectrum far from the edge (#1), a pair of conductance peaks with energy close to Δ are identified near the (11) edge (dashed lines in Figure S9d). Similar conductance peak can be obtained near the (01) edge (Figures S9b and S9e). Here, we want to point out that such conductance peak is not related to topological properties, but is a natural consequence of the reduction in superconducting gap magnitude, which can be reproduced by Dynes formula. Figure S9f shows two spectra simulated by Dynes formula with an anisotropic gap function (See Supplementary Note 1 for details). Based on the evolution of gap magnitude near the edges (Figures S1d and S1e), Δ_0 = 12 and 10 meV are used to mimic the tunneling spectra away from (red) and near (blue) the edge, respectively. The conductance peak indicated by dashed lines emerge naturally after subtracting the red spectrum from the blue spectrum (Figures S9g). Therefore, great care should be taken in determining pairing symmetry using the spectral weight obtained by such normalization method.

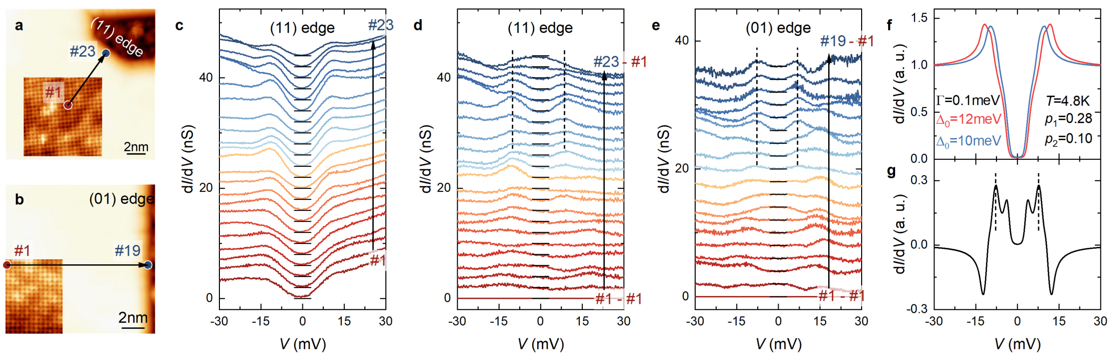

Figure S9 | Spectral weight of the normalized tunneling spectra. a-b, STM topographic images (V_s = 1 V, I_t = 50 pA) of the (11) and (01) edges. Insets: atomically resolved images (V_s = 50 mV, I_t

= 500 pA). **c-d**, Raw and normalized spectra collected along the black arrow in **a**. **e**, Normalized spectra collected along the arrow in **b**. **f**, Spectra with different gap values simulated by Dynes formula, where T = 4.8 K and Γ = 0.1 meV. The red and blue curves mimic the tunneling spectra away from and near the edge, respectively. **g**, Normalized spectra obtained by subtracting the red spectrum from the blue spectrum in **f**.

Supplementary Note 6: Correlation between edge state and pairing symmetry

We note that a previous work (Ref. [7]) has investigated the topological properties of single-layer FeSe and discovered the 1D topological edge states at the M point of the Brillouin zone. It should be emphasized that our findings do not conflict with those in Ref. [7]. **Notice that the topological phase in Ref. [7] is associated with the spin-orbit coupling gap in the antiferromagnetic state, and the topological band lies ~ 100 meV below the Fermi surface, which is well beyond the energy window of the superconducting gap (~ 15 meV).** Therefore, the topological edge states revealed in Ref. [7] are not related to the specific properties of superconductivity and cannot reflect the relevant information of superconducting pairing. In contrast, our theoretical[4] and experimental works focus on the superconductivity near the Fermi energy and the possible topological edge/corner states located within the superconducting gap which are closely related to the details of pairing symmetry. According to our theoretical calculations[4], a sign-changed $s_{\pm}$-wave pairing leads to a second-order superconducting state at the (01) edge and at the corner between the (11) and $(1\bar{1})$ edges, while the sign-preserving *s*-wave state remains topologically trivial even in the presence of the inversion symmetric Rashba SOC. The tunneling spectra we collected at edges and corners exhibit full gap and substantial dip near the Fermi energy, respectively, demonstrating the absence of topologically non-trivial edge/corner modes within the superconducting gap, and thus providing solid evidence for the sign-preserving *s*-wave pairing in single-layer FeSe.

Reference

1. Wang, Z. *et al.* Close relationship between superconductivity and the bosonic mode in $Ba_{0.6}K_{0.4}Fe_2As_2$ and $Na(Fe_{0.975}Co_{0.025})As$. *Nat. Phys.* **9**, 42-48 (2012).
2. Chen, C. *et al.* Observation of discrete conventional Caroli-de Gennes-Matricon states in the vortex core of single-layer $FeSe/SrTiO_3$. *Phys. Rev. Lett.* **124**, 097001 (2020).
3. Zhang, Y. *et al.* Superconducting gap anisotropy in monolayer FeSe thin film. *Phys. Rev. Lett.* **117**, 117001 (2016).
4. Qin, S., Fang, C., Zhang, F.-C. & Hu, J. Topological superconductivity in an extended *s*-wave superconductor and its implication to iron-based superconductors. *Phys. Rev. X* **12**, 011030 (2022).
5. He, S. L. *et al.* Phase diagram and electronic indication of high-temperature superconductivity at 65 K in single-layer FeSe films. *Nat. Mater.* **12**, 605-610 (2013).
6. Ge, Z. Z., Yan, C. H., Zhang, H. M., Agterberg, D., Weinert, M. & Li, L. Evidence for *d*-wave superconductivity in single layer $FeSe/SrTiO_3$ probed by quasiparticle scattering off step edges. *Nano Lett.* **19**, 2497-2502 (2019).
7. Wang, Z. F. *et al.* Topological edge states in a high-temperature superconductor $FeSe/SrTiO_3(001)$ film. *Nat. Mater.* **15**, 968-973 (2016).